International Journal of Pharmaceutics 420 (2011) 341–349

Contents lists available at SciVerse ScienceDirect

International Journal of Pharmaceutics

journal homepage: www.elsevier.com/locate/ijpharm

Pharmaceutical Nanotechnology

Cationic solid lipid nanoparticles (cSLN): Structure, stability and DNA binding capacity correlation studies

S. Doktorovova[a,b], R. Shegokar[b], E. Rakovsky[c], E. Gonzalez-Mira[d], C.M. Lopes[a,e], A.M. Silva[f], P. Martins-Lopes[a], R.H. Muller[b], E.B. Souto[a,e,*]

[a] Institute of Biotechnology and Bioengineering, Centre of Genomics and Biotechnology, University of Trás-os-Montes and Alto Douro (IBB/CGB-UTAD), Vila-Real, Portugal
[b] Institute of Pharmacy, Department of Pharmaceutics, Biopharmaceutics & NutriCosmetics, Freie Universität Berlin, Berlin, Germany
[c] Department of Inorganic Chemistry, Faculty of Natural Sciences, Comenius University, Bratislava, Slovakia
[d] Department of Physical Chemistry, Faculty of Pharmacy, University of Barcelona, Barcelona, Spain
[e] Faculty of Health Sciences, Fernando Pessoa University, Porto, Portugal
[f] Centre for the Research and Technology of Agro-Environmental and Biological Sciences, University of Trás-os-Montes and Alto Douro (CITAB-UTAD), Vila-Real, Portugal

ARTICLE INFO

Article history:
Received 5 July 2011
Received in revised form 24 August 2011
Accepted 26 August 2011
Available online 2 September 2011

Keywords:
Solid lipid nanoparticles
Gene delivery
Differential scanning calorimetry
Wide angle X-ray scattering
Stability studies

ABSTRACT

Cationic solid lipid nanoparticles (cSLN) are promising lipid nanocarriers for intracellular gene delivery based on well-known and widely accepted materials. cSLN containing single-chained cationic lipid cetyltrimethylammonium bromide were produced by high pressure homogenization and characterized in terms of (a) particle size distribution by photon correlation spectroscopy (PCS) and laser diffractometry (LD), (b) thermal behaviour using differential scanning calorimetry (DSC) and (c) the presence of various polymorphic phases was confirmed by X-ray diffraction (WAXD). SLN composed of Imwitor 900P™ (IMW) showed different pDNA stability and binding capacity in comparison to those of Compritol 888 ATO™ (COM). IMW-SLN, having *z*-ave = 138–157 nm and *d*(0.5) = 0.15–0.158 μm could maintain this size for 14 days at room temperature. COM-SLN had *z*-ave = 334 nm and *d*(0.5) = 0.42 μm on the day of production and could maintain similar size during 90 days. IMW-SLN revealed improved pDNA binding capacity. We attempted to explain these differences by different interactions between the solid lipid and the tested cationic lipid.

1. Introduction

Solid lipid nanoparticles (SLN) are versatile colloidal carriers being currently explored for administration routes (e.g. parenteral, oral, topical, dermal and transderaml) (Souto and Müller, 2007). Their advantage over colloidal carriers composed of polymers or inorganic material is the use of biocompatible lipids with well-established use in pharmaceuticals, e.g. glycerols with fatty acids, free fatty acids, fatty alcohols or waxes. This makes these systems closer to real-life use (Souto et al., 2011). Distinct advantage of SLN over polymeric nanoparticles is that SLN can be produced without use of organic solvents, using high pressure homogenization (HPH) method that is already successfully implemented in pharmaceutical industry.

Cationic SLN (cSLN), i.e. SLN containing at least one cationic lipid, have been proposed as non-viral vectors for gene delivery (Bondi and Craparo, 2010). The use of cSLN in this application is already quite well proven – it has been shown that cSLN can effectively bind nucleic acids, protect them from DNAase I degradation and deliver them into living cells (Bondi et al., 2007; Vighi et al., 2007; Xue and Wong, 2011). First proof of *in vivo* efficiency of SLN has also been reported (del Pozo-Rodríguez et al., 2010). A review of materials, production methods and *in vitro* testing has been reviewed by Bondi and Craparo (2010).

Although efficacy in DNA/RNA delivery into living cells has been satisfactorily proven (Bondi and Craparo, 2010; del Pozo-Rodríguez et al., 2010), there are still many features that need to be explained. Hardly predictable stability and polymorphic transformations of SLN have been related to their solid state (Bunjes, 2010). These features may have an impact on their use in future medicines. The same holds true for cSLN. In this study, we focused on cSLN containing one cationic lipid with a single hydrocarbon chain. We attempted to correlate physicochemical characteristics of the developed

Abbreviations: CMC, critical micelle concentration; COM, Compritol 888 ATO; CTAB, cetyltrimethylammonium bromide; HLB, hydrophilic–lipophilic balance; IMW, Imwitor 900; LD, laser diffraction; MIR, Miranol Ultra C-32; PCS, photon correlation spectroscopy; Polox, Poloxamer 188; SLN, solid lipid nanoparticles; T_m, melting temperature; *z*-ave, *z*-average (intensity weighed diameter); ZP, zeta potential.

* Corresponding author at: Faculty of Health Sciences of Fernando Pessoa University, Rua Carlos da Maia, 296, P-4200-150 Porto, Portugal. Tel.: +351 22 507 4630; fax: +351 22 550 4637.
E-mail addresses: eliana@ufp.edu.pt, souto.eliana@gmail.com (E.B. Souto).

0378-5173/$ – see front matter © 2011 Elsevier B.V. All rights reserved.
doi:10.1016/j.ijpharm.2011.08.042

Table 1
Composition of three different cationic solid lipid nanoparticles formulations prepared using high pressure homogenization.

Formulation	Solid lipid %(w/w)		CTAB %(w/w)	Surfactant %(w/w)	
	IMW	COM		Polox.	MIR
SLN-A	5.0		0.5	0.25	
SLN-B	5.0		0.5		0.25
SLN-C		5.0	0.5	0.25	

systems with their stability, which is a key issue for potential medicine, and DNA-binding. HPH has been used to produce cSLN because of its high reproducibility, scale-up feasibility and suitability for use in pharmaceutical production (Shegokar et al., 2011). Differential scanning calorimetry in combination with X-ray diffraction was used for an in-depth physicochemical characterization of SLN, especially focusing on solid state.

2. Materials and methods

2.1. Materials

Cetyltrimethylammonium bromide (CTAB) was acquired from Sigma (Sintra, Portugal). Imwitor 900P™ (IMW, 40–50% glyceryl monostearate) and Lutrol F68™ (F68, poly(ethylene oxide)–poly(propylene oxide)–poly(ethylene oxide); Poloxamer 188) were gifts from Sasol GmbH, Germany. Compritol 888 ATO™ (COM, glyceryl tribehenate) was donated by Gattefosse, France. Miranol Ultra C-32™ (MIR, sodium cocoamphoacetate) was obtained as gift sample from Condea GmbH. Trehalose was obtained from Merck (Darmstadt, Germany). All other reagents were from Sigma (Sintra, Portugal). Ultrapure water from MilliQ system (Millipore, Schwalbach, Germany) filtered by a filter with 0.22 μm pore size was used throughout the work. All materials were used as received.

2.2. Solid lipid nanoparticles production

SLN were produced by hot high pressure homogenization method (Shegokar et al., 2011). Briefly, lipid phase, consisting of solid lipid (either IMW or COM) and CTAB, was heated up to a temperature about 10 °C higher than the melting point of the solid lipid used, i.e., 70 °C for IMW-SLN and 80 °C for COM-SLN. Aqueous solution of surfactant (MIR or F68) was simultaneously heated to the same temperature. The lipid phase was dispersed in the aqueous phase using an Ultra Turax (IKA GmbH, Germany) for 30–60 s at 8000 rpm. This pre-emulsion was then homogenized using a LAB 40 homogenizer (40 ml; APV, Germany) operating at 500 bar for 3 homogenization cycles in discontinuous mode. The samples were filled in glass vials and let to cool down at room temperature. The composition of SLN is given in Table 1.

2.3. Particle size analysis

Size distribution analysis was performed by photon correlation spectroscopy (PCS) and laser diffraction (LD). PCS measurements were performed using a Zetasizer Nano ZS90 (Malvern Instruments, United Kingdom). Each sample was diluted with MiliQ water (0.5%, v/v) to obtain a weak opalescent dispersion and measured at 25 °C. The results are presented as intensity weighted average (*z*-ave) value obtained from three measurements (10 runs each) with corresponding standard deviation. Mastersizer 2000 equipped with Hydro 2000S sample dispersion unit (Malvern Instruments, United Kingdom) was used for LD measurements. Volume weighed diameter of 50% of particle population ($d(0.5)$) is given as a mean of 5 measurements with corresponding standard deviation. Stirrer speed was set to 2000 rpm to avoid particle aggregation during the measurement.

2.4. Zeta potential

Zeta potential was determined by laser Doppler anemometry using Smoluchowski model. All measurements were performed on Zetasizer Nano ZS90 using Dispersion Technology Software 5.1 in General Purpose mode and automatic measurements settings. MiliQ water adjusted to conductivity of 50 μS cm^{-1} (by addition of few droplets of 150 mmol sodium chloride solution) was used for sample dilution to weak opalescence (0.5%, v/v).

2.5. Differential scanning calorimetry

Differential scanning calorimetry (DSC) was performed using a Mettler DSC 821^e (Mettler Toledo) at heating rate of 5 K/min. Samples were accurately weighed into standard 40 μl aluminium pans and sealed; an empty sealed pan was used as a reference. Bulk IMW, COM, CTAB and all SLN formulations were used without any prior thermal treatment or other processing and directly weighted into the pans. The physical mixtures of IMW + CTAB and COM + CTAB were melted and allowed to solidify before the measurements. Data were processed using Star^e software 8.10. Recrystallization index (RI) was determined using the following equation (Freitas and Müller, 1999):

$$\mathrm{RI}\,[\%] = \frac{\Delta H(\mathrm{SLN})[\mathrm{J\ g^{-1}}]}{\Delta H(\mathrm{bulk})[\mathrm{J\ g^{-1}}] \cdot C(\text{lipid phase})} \times 100$$

where ΔH is the enthalpy (J g^{-1}) of SLN of bulk lipid and C is the concentration of lipid phase (%, w/w). Solid lipid (IMW or COM) was considered as lipid phase only.

2.6. X-ray diffraction

X-ray diffraction studies of bulk materials were performed on Bruker D8 Advance diffractometer with Copper anode (λ = 0.154056 nm) and LynxEye detector. Diffractograms were recorded between 2θ = 15–40° with a step of 0.04° and count time of 5 s. Samples were used without any prior thermal treatment or further processing. SLN samples were filled into sample holder with xanthan gum in an amount sufficient to form a thick paste.

2.7. Determination of DNA binding capacity

To compare the DNA binding capacity of the developed SLN formulations, SLN were mixed with model pDNA (2 μg/μl) in ratios of SLN:pDNA = 10, 20, 30, 40 and 50:1, w/w. Plasmid DNA was added into diluted SLN dispersions (0.1–0.5%, v/v, in ultrapure water), vortexed gently (3 s) immediately and allowed to form complexes at room temperature (25 °C) under mild shaking during 45 min. Size and zeta potential of resulting complexes were checked as stated above. All experiments were performed in triplicate with different pDNA stocks.

2.8. Gel-retardation assay

Immobilization of pDNA on SLN was verified by gel retardation assay (Vighi et al., 2007). 20 μl of each pDNA–SLN complex was mixed with 5 μl loading buffer (0.25%, w/w, bromophenol blue in TE buffer) and applied to 1.0% agarose gel. Electrophoresis was carried out at 80 V for 60 min at room temperature in 1× TAE buffer (40 mM Tris acetate and 1 mM EDTA). The gels were stained with 7 μg ml^{-1} ethidium bromide solution for DNA visualization.

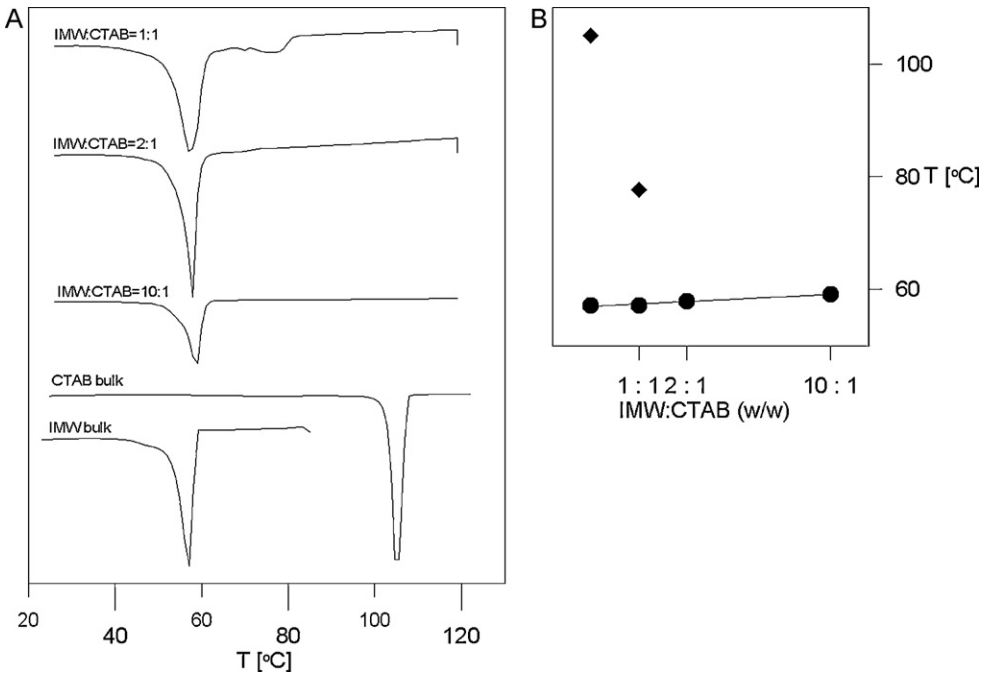

Fig. 1. (A) DSC thermograms of bulk IMW, bulk CTAB and physical mixtures of IMW and CTAB. (B) T_m dependence on IMW:CTAB weight ratio. ●*T* of occurrence of first melting event (melting of IMW), ♦*T* of occurrence of second melting event.

Images were captured with Gel Doc XR+ documentation system with ImageLab software (BioRad).

3. Results and discussion

3.1. Characterization of bulk materials and physical mixtures of bulk materials

Fig. 1 shows DSC thermograms and Fig. 2 X-ray diffractograms of bulk IMW, CTAB, and physical mixtures of these materials in given ratios. The melting temperatures of bulk IMW and CTAB were found at expected values of 59.18 °C and 105.89 °C, respectively

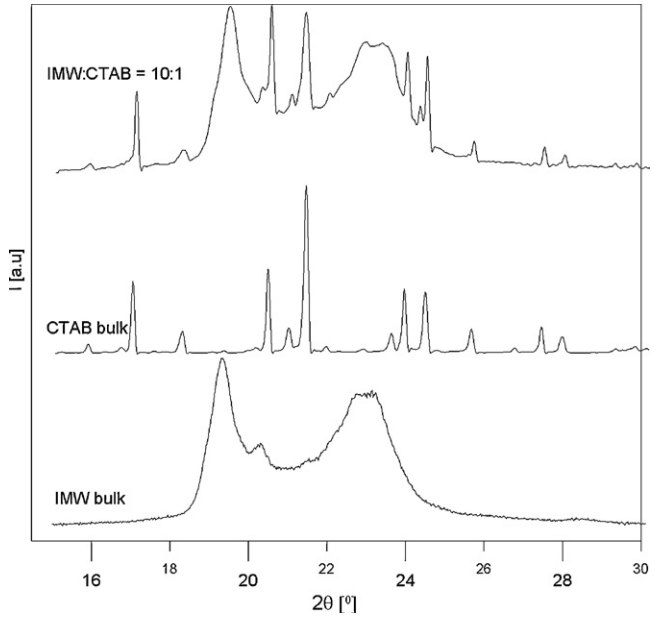

Fig. 2. X-ray diffraction patterns of (from top to bottom) physical mixture IMW:CTAB = 10:1, bulk CTAB, bulk IMW.

(Aleekseev et al., 2010; Müller et al., 2008). For the evaluation of crystallinity of SLN, the second heating run is taken into consideration, because the material in SLN has already undergone a heat stress during the production (Müller et al., 2008). Therefore, two heating runs were performed with bulk materials as well, the curves shown in Fig. 1 represent the 2nd heating run. IMW, an industrial grade mixture of monoacylglycerides (40–55%) and diglycerides (up to 40%) (IMWITOR® Glyceryl Stearates, 2008), crystallizes in α-modification but undergoes transformation into β-polymorph. This was detected in the 1st heating run, confirmed by the X-ray diffractogram showing several unresolved reflections at d = 0.45–0.46 nm (Krog, 2001). After first heating run, a small shift of melting temperature (T_m) indicates recrystallization in α-modification. Smaller peak area might be due to incomplete recrystallization after the first heating run.

CTAB generally shows 2 minor melting events below 100 °C, resulting from melting of acyl chains and a main transition at around 112 °C corresponding to complete melting of CTAB including the head-groups (Aleekseev et al., 2010). In our work, only a minor peak at 75.23 °C was detected, attributed to higher heating rate applied in this study. The thermal stress did not significantly affect the CTAB melting behaviour.

The physical mixtures of IMW and CTAB were studied at the ratio used in SLN (IMW:CTAB = 10:1) and at higher ratio IMW:CTAB = 2:1 and IMW:CTAB = 1:1 to assure that the response of CTAB lies within sensitivity limits of the methods used. X-ray diffractogram of physical mixture consisting of IMW:CTAB = 10:1 contains both reflections of β-polymorph of IMW and all reflections of CTAB except for reflections between $2\theta = 23°$ and 24° which have lower intensity than those originating from IMW. Interestingly, a small shift of T_m of the mixture in comparison of bulk IMW towards higher temperature was observed. No melting peak of CTAB was detected in this mixture. Attempts were made to measure bulk mixture without previous thermal treatment; the resulting DSC runs were similar to those of melted mixture, i.e. without any extra peak (data not shown). Further we analyzed the physical mixtures with higher CTAB content. Physical mixture of IMW:CTAB in 2:1 shows melting peak of IMW only as well. The thermogram of 1:1 mixture

Table 2
Summary of HLB and thermal characteristics of bulk material used for SLN production, (a) 1st heating run, and (b) 2nd heating run.

Sample	Composition	HLB		Integral [mJ]	Onset [°C]	Peak [°C]	Enthalpy [J g^{-1}]
IMW	Glycerylmonostearate 40–55%	3	(a)	−211.96	53.89	59.18	−176.34
	Glyceryldistearate 30–45%		(b)	−133.18	52.84	57.17	−110.80
COM	Glyceryldibehenate 40–60%	2	(a)	−201.31	69.70	72.05	−112.59
	Glyceryltribehenate 21–35%		(b)	−208.41	69.18	72.11	−116.56
CTAB	Cetyltrimethylammonium bromide 100%	10	(a)	−351.26	104.15	105.89	−154.67
			(b)	−346.84	103.06	105.04	−152.73

Table 3
Thermal characteristics of solid lipid–cationic lipid mixtures in various ratios. DSC parameters correspond to (a) 1st melting event and (b) 2nd melting event (if applicable).

IMW:CTAB		Integral [mJ]	Onset [°C]	Peak [°C]	Enthalpy [J g^{-1}]	COM:CTAB		Integral [mJ]	Onset [°C]	Peak [°C]	Enthalpy [J g^{-1}]
10:01	(a)	−216.64	55.38	59.15	−100.76	10:01	(a)	−218.54	68.31	71.49	−104.36
	(b)	n.a.	n.a.	n.a.	n.a.		(b)	−3.12	96.42	99.82	−1.49
02:01	(a)	−150.28	55.45	57.98	−79.52	02:01	(a)	−159.48	66.68	69.65	−71.20
	(b)	n.a.	n.a.	n.a.	n.a.		(b)	−16.32	96.15	96.98	−7.29
01:01	(a)	−133	52.63	57.24	−61.57	01:01	(a)	−119.92	64.25	68.82	−61.50
	(b)	−12.69	71.49	77.73	−5.88		(b)	−51.47	93.04	94.88	−26.39

depicts a second melting event immediately after IMW melting, with onset at 71.49 °C. The DSC data are summarized in Table 2 (bulk materials) and Table 3 (Physical mixtures).

Monoacylglycerides, which present 40–55% (w/w) of IMW composition, are amphiphilic compounds. Despite being used as solid lipid here they also have mild surfactant activity and some authors regard it rather as a surfactant than solid lipid (Bhalekar et al., 2009). The hydrophilic–lipophilic balance (HLB) of this mixture is 3, indicating a lipophilic character. CTAB is in general used as surfactant, owing to its structure with perfectly balanced hydrophilic and hydrophobic moieties (HLB = 10). For the purpose of gene delivery, molecules with structure containing a hydrophobic chain (either an aliphatic hydrocarbon chain or steroid), a linker and a polar, positive charge bearing head group are conventionally referred to as cationic lipids (Karmali and Chaudhuri, 2007). CTAB as bulk material has waxy appearance and a melting point well over 40 °C which lead to its use in some SLN formulations to provide positive surface charge (Cui and Mumper, 2002; Siddiqui et al., 2010). Mixtures of IMW and CTAB show that there is a strong interaction between these two materials. From the IMW:CTAB ratio 2:1 and higher (e.g. 10:1) CTAB does not exist in solid state. Also, the melting enthalpy of IMW is decreasing with increasing CTAB content, indicating lower crystallinity of these matrices. Taking into account HLB 10 of CTAB, it is expected to be located at oil–water interface during the production of SLN and act as surfactant in the resulting SLN dispersion.

Fig. 3 shows the DSC thermograms and Fig. 4 shows the X-ray diffraction patterns of bulk COM and physical mixtures of COM with CTAB in given ratios. The thermogram and diffractogram of bulk material show COM in β′ modification characterized by reflection at $2\theta = 21.21°$ ($d = 0.419$ nm) with a shoulder at $2\theta = 23.3°$ ($d = 0.381$) (Souto et al., 2006). T_m of this polymorph was found at expected temperature (Hamdani et al., 2003; Rahman et al., 2010; Souto et al.,

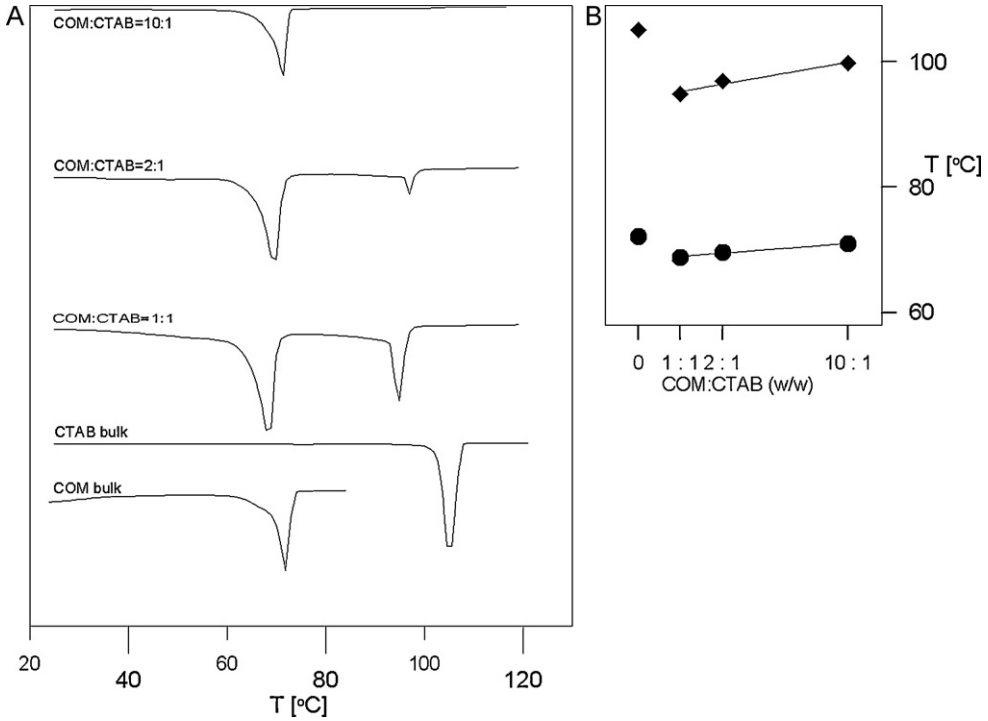

Fig. 3. (A) DSC thermograms of bulk COM, bulk CTAB and physical mixtures of COM and CTAB. (B) T_m dependence on COM:CTAB weight ratio. ●*T* of occurrence of first melting event (melting of IMW), ♦*T* of occurrence of second melting event (attributed to melting of CTAB).

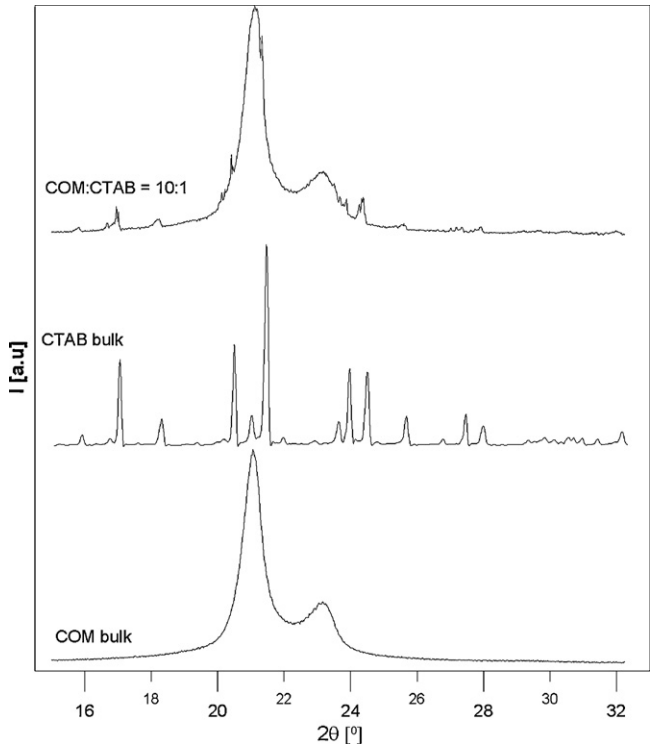

Fig. 4. X-ray diffraction patterns of (from top to bottom) physical mixture COM:CTAB = 10:1, bulk CTAB, bulk COM.

2006); small portion of α-polymorph might be present, resulting in a shoulder with T_{onset} = 69.18 °C (Brubach et al., 2007). A small increase of T_m after first heating cycle was also detected (Souto et al., 2006). Physical mixture of COM and CTAB in ratio 10:1 presented lower T_{onset} and T_m. This usually happens, when an impurity is introduced to the lipid crystal. Also, a tiny peak at T_m = 99.82 °C has been repeatedly detected. The area of this peak is about 1/10 of the area of COM. At higher COM:CTAB ratios, another distinct melting event with peak at 96.98 °C (2:1) and 94.88 °C (1:1) is well detected. Although these peaks are detected at temperatures −5 °C lower than T_m of bulk CTAB, they might be attributed to melting of CTAB. The peak temperature of this second event varies with COM:CTAB ratio – the highest T_m is observed in COM:CTAB 10:1 (see Fig. 2B). The area of the second melting event corresponds to the CTAB content in the mixture. T_m of COM shows only small changes depending on COM:CTAB ratio – the highest T_m is observed at 10:1 ratio. All reflections of CTAB are visible in diffractogram of COM:CTAB = 10:1 mixture, which further confirms the presence of CTAB in solid state (Fig. 4).

Compritol 888 ATO is a lipid mixture with well established use in SLN formulation (Bondi et al., 2007; Souto et al., 2006; Vighi et al., 2007). Mixtures with CTAB show that the solid lipid and cationic lipid form a heterogeneous mixture, not uncommon for a mixture of two lipids (Souto et al., 2006). There is no complete phase separation; and the enthalpy of the melting peaks is proportional to the weight ratio of the lipids. This behaviour is very similar to oil-solid lipid matrices found in nanostructured lipid carriers (NLC) – the crystallinity of the solid lipid is reduced, but the lipid with lower content is not fully incorporated in the solid lipid (Souto et al., 2006). For a SLN formulation, this situation should be advantageous (providing higher stability with reduced rate of polymorphic transitions), but in this particular case CTAB (HLB = 10) should not be expected to behave as solid lipid (see further).

Table 4
Optimization of number of homogenization cycles for production of cationic SLN by hot HPH and the particle size obtained.

Formulation	PCS		LD (μm)		
	z-ave (nm)	PdI	*d*(0.500)	*d*(0.900)	*d*(0.950)
SLN-A					
1 cycle[a]	162 ± 4	0.326	0.160	1.622	22.213
2 cycles[a]	133 ± 1	0.421	0.149	0.914	5.543
3 cycles[a]	131 ± 11	0.390	0.162	46.154	98.479
SLN-B					
1 cycle[a]	219 ± 4	0.273	0.213	21.770	32.406
2 cycles[a]	172 ± 3	0.339	0.177	14.049	41.356
3 cycles[a]	139 ± 4	0.361	0.168	25.184	63.453

[a] Homog. cycles.

3.2. Production and size distribution analysis

Cationic SLN were produced by hot HPH. The optimized formulations composition is listed in Table 1. HPH is considered the most advantageous method for SLN production because of its high efficacy in particle size and polydispersity reduction, readily available scale-up possibilities and established use in pharmaceutical industry (Shegokar et al., 2011). Three cycles at 500 bars have been selected as optimal production parameters, as a decrease of the mean size with increasing cycle numbers was observed. At the same time, increase of particle aggregation was represented by slightly higher *z*-ave and significantly higher *d*(0.95) and *d*(0.99) value were observed (Table 4). Therefore, further increasing of number of cycles would compromise the quality of the resulting dispersion. Average particle size distributions of 3 batches, produced from the same starting materials, by the same devices and on the same day, are given in Table 5. Small populations (e.g., SLN-A 1.39% of volume) of particles with diameter >1 μm have been detected by LD already on the day of production, their presence is also reflected by polydispersity values of ∼0.4. Application of higher pressure (1000 bar, 3 cycles) did not improve SLN characteristics – both IMW-based formulations yielded particles with *z*-ave in micrometer range; COM-SLN-C had approximately the same characteristics as when produced at 500 bar (Table 4).

3.3. Surface charge estimation

All SLN formulations showed high positive zeta potential (ZP) values, indicating that electrical repulsion will contribute to stabilization of the systems. Highly positive ZP is also a pre-requisite for sufficient pDNA binding (Bondi and Craparo, 2010). The average values of ZP obtained from three independent batches are given in Table 5. SLN-C showed unimodal ZP distribution, while SLN-A and SLN-B showed up to 3 peaks in ZP distribution, which is also reflected by higher standard deviations.

CTAB readily associates with colloidal surfaces consisting of various materials, which is reflected by rise in ZP, often from negative values, when compared to the same material in absence of CTAB. CTAB associated with cetylalcohol SLN in presence of polysorbate 60 could give ZP as high as 60–65 mV (Cui and Mumper, 2002). The values reported here are similar to those already published, especially to the systems consisting of solid lipid + cationic lipid + surfactant. The use of another surfactant shields the high ZP

Table 5
Particle size distribution and zeta-potential of SLN on the day of production.

	z-ave (nm)	PdI	*d*(0.500) (μm)	ZP (mV)
SLN-A	138 ± 0	0.430	0.150	63.9
SLN-B	157 ± 5	0.336	0.158	59.6
SLN-C	334 ± 18	0.429	0.420	68.8

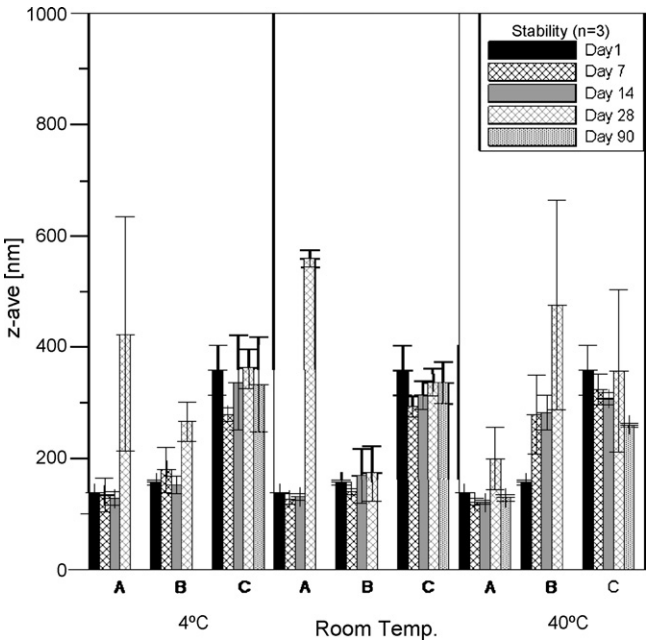

Fig. 5. PCS-average size of SLN-A, SLN-B and SLN-C at different storage conditions during 90 days after production ($n = 3$).

provided by CTAB to some extent. Poloxamer 188 alone as a stabilizer provides negative charge to the particle surface, as in contact with the aqueous phase the poly(ethylene oxide)–poly(propylene oxide)–poly(ethylene oxide) (PEO–PPO–PEO) block structure is the one with smaller dielectric constant in comparison to water; the resulting charge relative to water will be negative (Rosen, 2004). The same explanation applies to Miranol C-32 Ultra-stabilized SLN-B. The ZP of SLN-B was the lowest among the three formulations reported here, indicating that the effect of MIR is more pronounced than the effect of Poloxamer 188.

3.4. Short term stability testing

Stability is a crucial factor for practical use of any pharmaceutical formulation. For stability testing, 3 batches of each SLN formulation were stored in transparent glass vials at 4 °C, room temperature (23 ± 2 °C) and 40 °C. Particle size was monitored by PCS and LD measurements at selected time intervals. The average intensity weighted diameters (*z*-ave) and polydispersity indices from three batches per formulation are given in Table 6 and Fig. 5. SLN-A showed minimal changes in particle size up to 14 days, a sharp increase of *z*-ave was observed on day 28 in samples stored at room temperature and 4 °C. Simultaneously, sedimentation was also observed. Interestingly, SLN-A stored at 40 °C remained stable during the entire observed period of 90 days, maintaining *z*-ave slightly below *z*-ave on the day of production and showing no visible signs of instability. Average size of SLN-B was found to be gradually increasing over the first 28 days. Further long-term stability testing of this sample was discontinued after 50 days at all storage conditions due to marked increase in particle size and sedimentation and gel formation at 40 °C.

SLN-C, which has the largest average diameter of the presented formulations, showed the best stability – particle size remained similar to the original size determined on the day of production during the following 90 days.

All cSLN formulations were also tested for stability in human blood plasma after incubation at 37 °C for 5 min. All three formulations presented *z*-ave similar to the *z*-ave in original dispersion medium and marked increase of PdI to values of 0.911 (SLN-B) to 1.0 (SLN-C).

In case of cationic SLN, stability much lower than stability of negatively charged SLN has been reported. The longest stability of cationic SLN reported to this date is up to 180 days (Bondi et al., 2007; Montana et al., 2007) for cationic SLN of similar composition as our SLN-C (Compritol 888 ATO in combination of Pluronic F68 and one cationic lipid). Stability up to 30 days has been reported by other groups (Siddiqui et al., 2010; Vighi et al., 2007). In comparison to these results, stability of SLN-C may be considered acceptable, while stability of SLN-B and SLN-A (with exception of SLN-A stored at 40 °C which might not poses a solid matrix) may be considered as comparable to published formulations, but insufficient for practical use. We assume that different stability of SLN-A and SLN-B in contrast to SLN-C is governed by different structures of these SLN (see further).

Table 7
DSC data of cationic SLN. Heating rate of 5 K/min was used.

Formulation	Integral [mJ]	Onset [°C]	Peak [°C]	Enthalpy [J g^{-1}]	RI [%]
SLN-A	−107.96	52.52	56.02	−4.32	77.93
SLN-B	−102.19	54.16	58.47	−4.21	76.07
SLN-C	−113.80	68.78	74.65	−5.62	96.43

3.5. Structural analysis

Figs. 6 and 7 show DSC curves and X-ray diffractograms of SLN. The summary of DSC data is given in Table 7. SLN-A and SLN-B showed crystallinity of 77.98% and 75.99% (enthalpy of bulk IMW from second heating run was used), respectively. X-ray diffractograms show the typical reflection of α-modification of IMW, but followed by two extra reflections at $2\theta = 19.81°$ and 23.01°, which are not consistent with α-polymorph but occur rather at angles typical for β-modification. The strongest reflection of IMW at $2\theta = 21.38°$ overlaps the region of the two strongest reflection of CTAB at $2\theta = 21.48°$ and 20.51°, however, the other reflections at

Table 6
Comparative stability data of three different cationic SLN formulations stored at different conditions.

	SLN	Day 7		Day 14		Day 28		Day 90	
		z-ave[nm]	PdI	*z*-ave[nm]	PdI	*z*-ave[nm]	PdI	*z*-ave[nm]	PdI
4 °C	A	134 ± 30	0.442	128 ± 12	0.421	424 ± 221	0.559	n.a.	n.a.
	B	180 ± 41	0.449	152 ± 16	0.376	266 ± 99	0.470	n.a.	n.a.
	C	279 ± 12	0.338	336 ± 85	0.474	362 ± 70	0.528	333 ± 85	0.534
Room temperature	A	127 ± 9	0.410	131 ± 6	0.444	559 ± 530	0.606	n.a.	n.a.
	B	141 ± 5	0.342	168 ± 48	0.405	173 ± 30	0.404	n.a.	n.a.
	C	294 ± 19	0.396	313 ± 26	0.429	337 ± 76	0.408	337 ± 38	0.467
40 °C	A	122 ± 6	0.377	121 ± 4	0.555	200 ± 58	0.506	129 ± 6	0.362
	B	279 ± 12	0.602	282 ± 31	0.379	476 ± 231	0.659	n.a.	n.a.
	C	325 ± 27	0.637	308 ± 12	0.692	357 ± 59	0.508	261 ± 4	0.470

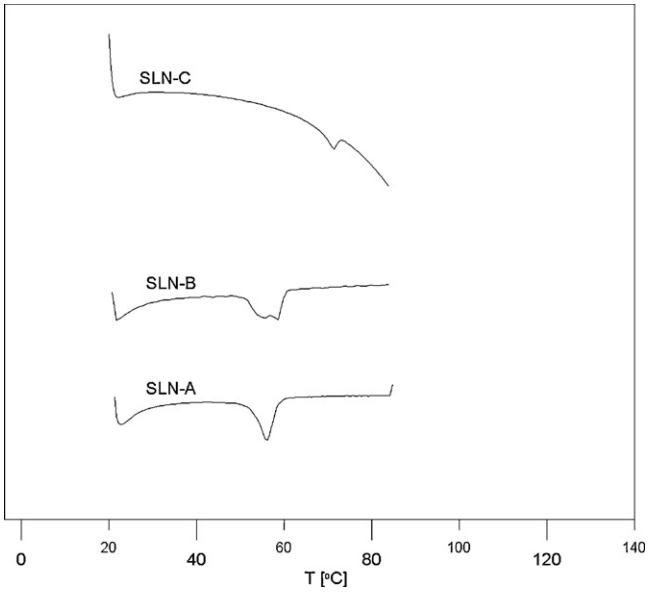

Fig. 6. DSC thermograms of SLN. From top to bottom: (a) SLN-A, (b) SLN-B, (c) SLN-C.

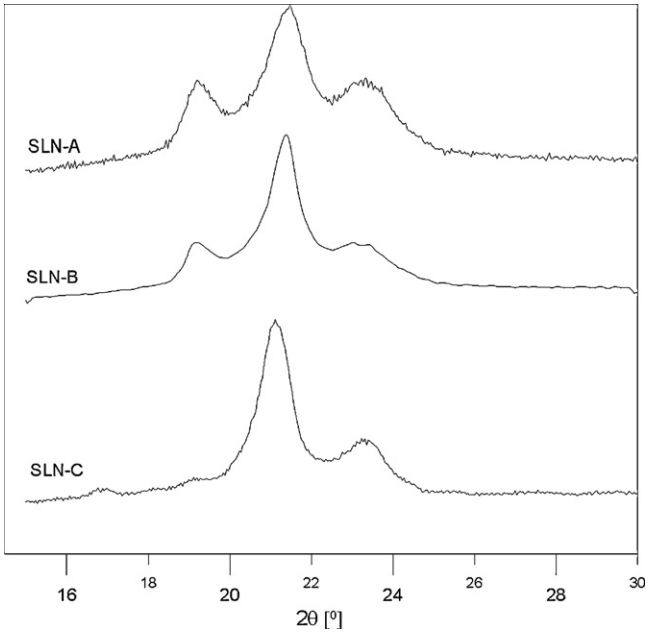

Fig. 7. X-ray diffraction patterns of SLN. From top to bottom: (a) SLN-A, (b) SLN-B, (c) SLN-C.

$2\theta = 17.06^\circ$, 23.64° and 23.97° are not present in the diffractogram of SLN-A nor SLN-B. T_m of SLN-A and SLN-B is shifted to a lower temperature in comparison to T_m of IMW:CTAB = 1:10, which might be attributed to decrease of T_m related to decrease of size of the material (i.e., increase in surface curvature). However, a larger T_m shift would be expected with respect to the mean diameter of these systems – typically 3–4 °C shift is observed in SLN with comparable size (Bunjes and Unruh, 2007; Vighi et al., 2007). In the case of SLN-A and SLN-B, we anticipate that IMW is present in both α and β polymorphs (note that monoacylglycerides–diglycerides mixtures usually do not form β′ form (Krog, 2001)), indicating ongoing polymorphic transitions already at first days after production. This could also explain the stability of SLN-A and SLN-B and a gradual increase of size and PdI as soon as 14 days after production. Low crystallinity resulting from low percentage of recrystallized lipid might be the reason of weak T_m shift to lower temperature. CTAB in presence of Poloxamer block copolymers forms various colloidal structures; their existence is concentration dependent (Ivanova et al., 2001). As critical micellar concentration (CMC) of CTAB and Poloxamer 188 in the presence of IMW is unknown, existence of other colloidal structures apart from SLN (as confirmed by DSC) with CTAB on the surface is obvious. This is also supported by bimodal ZP distribution, indicating various populations of positively charged colloidal structures in the dispersion.

A different behaviour has been observed for COM-based samples. Melting temperature of SLN-C is practically the same as T_m of physical mixture (71.4 °C vs. 71.49 °C). The diffractogram of SLN-C shows COM in its stable β′ phase, with a higher noise/small shoulder at around $2\theta = 19^\circ$. At this wavelength a shoulder appears in aged COM samples i.e. after storage at temperature of 40 °C or 50 °C for several weeks (Hamdani et al., 2003). We were unable to detect any reflections of CTAB, but a higher noise around $2\theta = 17^\circ$ and a broader shoulder at $2\theta = 24^\circ$ are usually not found in drug-free, Poloxamer-stabilized COM-SLN. Due to low concentration of CTAB used and the fact that a semisolid sample with amorphous matrix is measured, detection of response from CTAB is challenging. Therefore, we assume that COM is present in β or β′ polymorph already shortly after production, which might clarify the long-term stability of COM-SLN both in our work and in already published reports (Bondi et al., 2007; Montana et al., 2007). The mean diameter of particles (*z*-ave) was not constant during the observed time period, but always very similar to *z*-ave measured on the day of

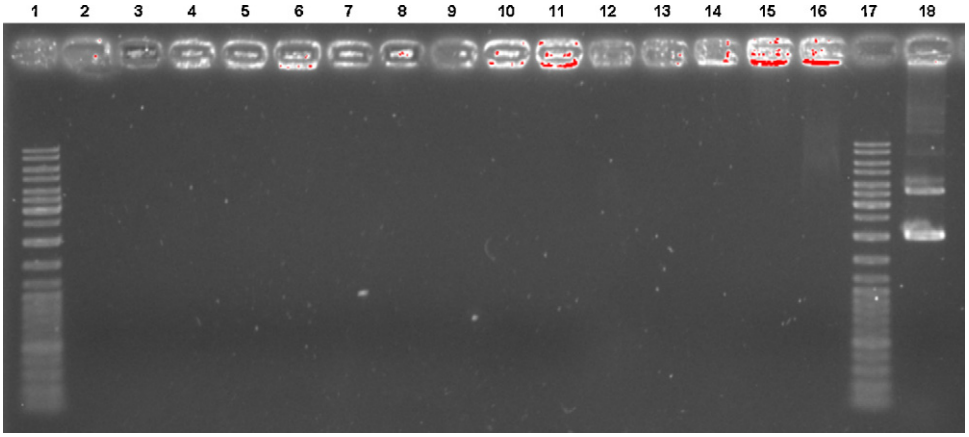

Fig. 8. Gel retardation assay. From left to right: (1) DNA ladder, (2)–(6) SLN-A:pDNA in ratios 50, 40, 30, 20, 10:1 (w/w), (7)–(11) SLN-B:pDNA in ratios 50, 40, 30, 20, 10:1 (w/w), (12)–(16) SLN-C:pDNA in ratios 50, 40, 30, 20, 10:1 (w/w), (17) DNA ladder, (18) free pDNA.

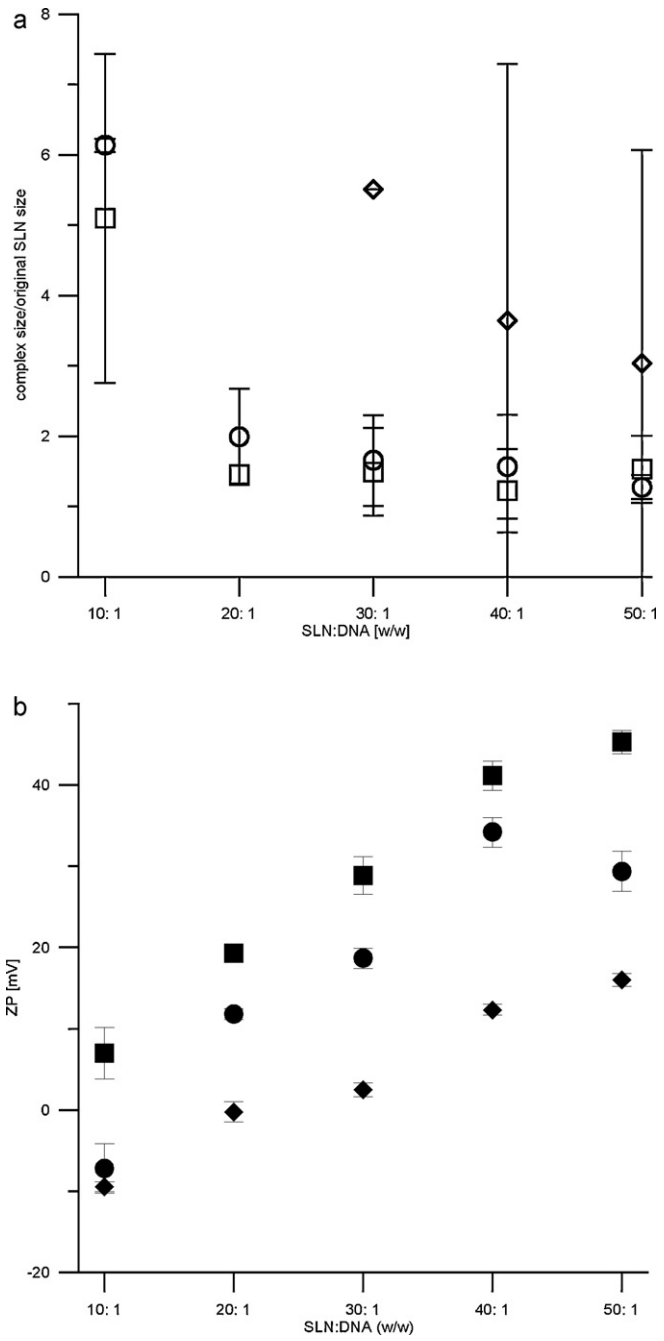

Fig. 9. Physicochemical characteristics of pDNA–SLN complexes. (A) (top): Size ratio ($z\text{-ave}_{(pDNA+SLN)}$:$z\text{-ave}_{(SLN)}$) ○ SLN-A, □ SLN-B, ◊ SLN-C; (B) (bottom) ZP of pDNA–SLN. ● SLN-A, ■ SLN-B, ♦ SLN-C.

production (Table 6). Furthermore, CTAB presence in solid state was clearly observed in physical mixture; unfortunately no conclusion on CTAB state/localization can be driven from the XRD and DSC curves of SLN-C. In any case, these curves show slight differences from negatively charged SLN with equivalent composition (5% (w/w) or more of Compritol 888 ATO, 1.2% (w/w) or more of Poloxamer 188) (Freitas and Müller, 1999; Souto et al., 2006). SLN with this composition are well known for their excellent physical stability. Addition of ionic surfactant should further increase their stability. Also, the equivalent SLN without CTAB usually show ZP below −30 mV, highly positive ZP in the formulation reported here confirms CTAB association with the particle surface.

Integration of cationic lipid into solid lipid core was proposed for Esterquat (N,N-di-(β-stearoylethyl)-N,N-dimethyl-ammonium chloride) and stearylamine modified stearic-acid based SLN with similar thermal behaviour (Vighi et al., 2007). However, as doubts exist about the actual possibility of incorporating oil or another solid lipid into the solid lipid core (Bunjes, 2010), this model should be critically evaluated. The thermograms here show phase separation of the solid lipid and cationic lipid. Another fact is that the SLN formulations were produced in a dispersion at only 5% (w/w) solid lipid at a temperature below T_m of CTAB, i.e. CTAB is rather adsorbed on the particle surface. The presence of CTAB in solid state is unlikely. Existence of other colloidal structures is also possible here, but ZP measurements of SLN-C revealed highly positive charge and unimodal ZP distribution.

3.6. Determination of pDNA-binding capacity

Fig. 8 shows agarose gel after gel retardation assay of pDNA–SLN complexes formed at given weight ratios. The lane on the right shows native pDNA. As can be seen in this figure, except from SLN-C at 10:1 ratio, all complexes could prevent the pDNA from migration in electric field, proving its successful coupling with SLN. Fig. 9 shows the ratio of complex size vs. original size and ZP of resulting complexes. Both IMW-SLN formulations could immobilize pDNA already at 10:1 (w/w) ratio; at 30:1 and higher the resulting complex size was similar to original size and ZP was maintained above 30 mV which should guarantee colloidal stability of the complex. The COM-SLN-C immobilized pDNA at weight ratio of 20:1; complex size and ZP were acceptable only at 50:1 ratio. No significant differences between Poloxamer 188-stabilized SLN-A and Miranol-stabilized SLN-B were observed. It was expected that binding capacity will be governed by surface characteristics of the particles, i.e. by the surfactant layer composition. In reality, a similar pDNA binding capacity was showed by IMW-SLN, better than COM-SLN. The reason of this behaviour might be the interaction between CTAB and the solid lipid – as stated above, loose interaction of CTAB with IMW is expected; and contribution of another colloidal species is also considered. CTAB, localized at any surface in this dispersion, is readily available to bind pDNA. In the other case, a stronger interaction between pDNA and cationic lipid seems to be shielded by the Poloxamer layer. The concentration of CTAB in this formulation was the same, which suggests that some portion of CTAB in the dispersion is not available for pDNA binding.

4. Conclusions

We have found differences between pDNA binding capacity of presented cationic SLN, which appear to be related not to surfactant, but to solid lipid–cationic lipid combination forming the SLN. IMW-SLN, both Poloxamer and Miranol-stabilized, showed better pDNA binding capacity. The drawback of these formulations is their stability limited to maximally 15 days. This already allows performing some *in vitro* experiments, but is definitely insufficient for a nanocarrier-based medicine. Despite IMW owning some surfactant properties, the resulting particles do posses solid matrix. The polymorphic transitions occur already few days after production. From the very first hours after production, samples tend to aggregate. Size of these SLN begins increasing already at day 15 after production, which is also accompanied by first signs of sedimentation, and presence of particles with size in micrometer range. The cationic lipid present at SLN surface might be bound very loosely and desorbs from the surface with time. Excess of CTAB might form another forms of colloidal species, which will also contribute to DNA binding.

COM-SLN, based on already well proven SLN formulation, have good (up to 90 days) physico-chemical stability which might be reinforced by the presence of cationic lipid. The ZP of the formulation was decreasing at smaller rate than that of IMW-SLN. The resulting stability is comparable to frequently reported stability of negatively charged SLN, but is still insufficient for practical use. On the other hand, the binding capacity of pDNA is lower than IMW-SLN, indicating that a lower portion of CTAB is available for formation of complex with pDNA.

The implications for design of "optimal" cationic SLN, i.e. with sufficient stability comparable to normal SLN, but with good capacity to bind DNA, it seems important to consider the combination of solid lipid–cationic lipid to assure good binding capacity and high stability. The combination in which the solid lipid which mixes well with the cationic lipid but the crystalline state of cationic lipid is remained might contribute to formation of SLN with better stability than the combinations in which the cationic lipid is dissolved in the solid lipid. In the first case the cationic lipid might contribute to lipid matrix formation, in the second case the cationic lipid acts as a surfactant. The selection of other surfactant, if necessary, can be done with respect to the selected solid lipid, similarly to negatively charged SLN.

Acknowledgements

We would like to express our gratitude to Ms. Corinna Schmidt for technical assistance throughout the work and to Dr. Sonia Gomes for assistance with gel documentation system. We would also like to thank Ms. Andjelka Kovacevic for critical reading of this manuscript. Financial support of Portuguese Science and Technology Foundation (a doctoral grant ref. SFRH/BD/60552/2009 to SD) is gratefully acknowledged. The authors also acknowledge FCT, under the reference PTDC/SAU-FAR/113100/2009.

References

Aleekseev, O.M., Lazarenko, M.M., Puchkovska, G.O., Bezrodnaya, T.V., Sendzyuk, A.A., 2010. Peculiarities if the thermal motion in crystals formed by cetyltrimethylsmmonium bromide molecules. Ukr. J. Phys. 55, 973–979.

Bhalekar, M., Pokharkar, V., Madgulkar, A., Patil, N., Patil, N., 2009. Preparation and evaluation of miconazole nitrate-loaded solid lipid nanoparticles for topical delivery. AAPS PharmSciTech 10, 289–296.

Bondi, M.L., Azzolina, A., Craparo, E.F., Lampiasi, N., Capuano, G., Giammona, G., Cervello, M., 2007. Novel cationic solid-lipid nanoparticles as non-viral vectors for gene delivery. J. Drug Target. 15, 295–301.

Bondi, M.L., Craparo, E.F., 2010. Solid lipid nanoparticles for applications in gene therapy: a review of the state of the art. Expert Opin. Drug Deliv. 7, 7–18.

Brubach, J.B., Jannin, V., Mahler, B., Bourgaux, C., Lessieur, P., Roy, P., Ollivon, M., 2007. Structural and thermal characterization of glyceryl behenate by X-ray diffraction coupled to differential calorimetry and infrared spectroscopy. Int. J. Pharm. 336, 248–256.

Bunjes, H., 2010. Lipid nanoparticles for the delivery of poorly water-soluble drugs. J. Pharm. Pharmacol. 62, 1637–1645.

Bunjes, H., Unruh, T., 2007. Characterization of lipid nanoparticles by differential scanning calorimetry. X-ray and neutron scattering. Adv. Drug Deliv. Rev. 59, 379–402.

Compritol 888 ATO, 2011. Technical Data Sheet, Gattefosse. SAS, France.

Cui, Z., Mumper, R.J., 2002. Genetic immunization using nanoparticles engineered from microemulsion precursors. Pharm. Res. 19, 939–946.

del Pozo-Rodríguez, A., Delgado, D., Solinís, M.Á., Pedraz, J.L., Echevarría, E., Rodríguez, J.M., Gascón, A.R., 2010. Solid lipid nanoparticles as potential tools for gene therapy: in vivo protein expression after intravenous administration. Int. J. Pharm. 385, 157–162.

Freitas, C., Müller, R.H., 1999. Correlation between long-term stability of solid lipid nanoparticles (SLN(TM)) and crystallinity of the lipid phase. Eur. J. Pharm. Biopharm. 47, 125–132.

Hamdani, J., Moes, A.J., Amighi, K., 2003. Physical and thermal characterisation of Precirol™ and Compritol™ as lipophilic glycerides used for preparation of a controlled-release matric pellets. Int. J. Pharm. 260, 47–57.

IMWITOR® Glyceryl Stearates, 2008. Product Information. Sasol Germany, GmbH.

Ivanova, R., Alexandridis, P., Lindman, B., 2001. Interaction of poloxamer block copolymers with cosolvents and surfactants. Colloids Surf., A 183–185, 41–53.

Karmali, P.P., Chaudhuri, A., 2007. Cationic liposomes as non-viral carriers of gene medicines: resolved issues, open questions, and future promises. ChemInform 5, 696–722.

Krog, N., 2001. Crystallization properties and lyotropic phase behavior of food emulsifiers: relation to technical applications 505. In: Garti, N. (Ed.), Crystalization Processes in Fats and Lipid Systems. Macel Dekker.

Montana, G., Bondi, M.L., Carrotta, R., Picone, P., Craparo, E.F., San Biagio, P.L., Giammona, G., Di Carlo, M., 2007. Employment of cationic solid-lipid nanoparticles as RNA carriers. Bioconjug. Chem. 18, 302–308.

Müller, R.H., Runge, S.A., Ravelli, V., Thünemann, A.F., Mehnert, W., Souto, E.B., 2008. Cyclosporine-loaded solid lipid nanoparticles (SLN®): drug-lipid physicochemical interactions and characterization of drug incorporation. Eur. J. Pharm. Biopharm. 68, 535–544.

Rahman, Z., Zidan, A.S., Khan, M.A., 2010. Non-destructive methods of characterization of risperidone solid lipid nanoparticles. Eur. J. Pharm. Biopharm. 76, 127–137.

Rosen, M.J., 2004. Emulsification by surfactants. In: Rosen, M.J. (Ed.), Surfactants and Interfacial Phenomena. , 3rd ed. John Wiley and Sons, Hoboken, New Jersey, pp. 303–332.

Shegokar, R., Singh, K.K., Müller, R.H., 2011. Production & stability of stavudine solid lipid nanoparticles – from lab to industrial scale. Int. J. Pharm. 416, 461–470.

Siddiqui, A., Patwardhan, G.A., Liu, Y.-Y., Nazzal, S., 2010. Mixed backbone antisense glucosylceramide synthase oligonucleotide (MBO-asGCS) loaded solid lipid nanoparticles: in vitro characterization and reversal of multidrug resistance in NCI/ADR-RES cells. Int. J. Pharm. 400, 251–259.

Souto, E.B., Doktorovová, S., Boonme, P., 2011. Lipid-based colloidal systems (nanoparticles, microemulsions) for drug delivery to the skin: materials and end-product formulations. J. Drug Deliv. Sci. Technol. 21, 43–54.

Souto, E.B., Mehnert, W., Müller, R.H., 2006. Polymorphic behaviour of Compritol® 888 ATO as bulk lipid and as SLN and NLC. J. Microencapsul. 23, 417–433.

Souto, E.B., Müller, R.H., 2007. Lipid nanoparticles (SLN and NLC) for drug delivery. In: Domb, A.J., Tabata, Y., Ravi Kumar, M.N.V., Farber, S. (Eds.), Nanoparticles for Pharmaceutical Applications. American Scientific Publishers, Los Angeles, California, pp. 103–122.

Vighi, E., Ruozi, B., Montanari, M., Battini, R., Leo, E., 2007. Re-dispersible cationic solid lipid nanoparticles (SLNs) freeze-dried without cryoprotectors: characterization and ability to bind the pEGFP-plasmid. Eur. J. Pharm. Biopharm. 67, 320–328.

Xue, H.Y., Wong, H.L., 2011. Tailoring nanostructured solid-lipid carriers for time-controlled intracellular siRNA kinetics to sustain RNAi-mediated chemosensitization. Biomaterials 32, 2662–2672.